Si(100) surface morphology evolution during normal-incidence sputtering with 100–500 eV Ar^+ ions

F. Ludwig, Jr.[a)]
Department of Physics, Boston University, Boston, Massachusetts 02215

C. R. Eddy, Jr.
Department of Electrical and Computer Engineering, Boston University, Boston, Massachusetts 02215 and Naval Research Laboratory, Code 6861, Washington, DC 20375

O. Malis[b)] and R. L. Headrick[c)]
Cornell High Energy Synchrotron Source, Cornell University, Ithaca, New York 14853

(Received 22 April 2002; accepted 15 August 2002)

Grazing incidence small-angle x-ray scattering and atomic force microscopy have been used to systematically investigate the evolution of Si(100) surface morphology during normal-incidence Ar^+ sputtering as a function of ion energy in the range of 100–500 eV. For ion energy ranges of 100–300 eV, two structures with distinct individual length scales and behaviors form on the surface. There is a smaller scale (lateral size of 20–50 nm) morphology that grows in scattering intensity and coarsens with time. There is also a larger scale (lateral size of approximately 100 nm) morphology that grows in scattering intensity but does not coarsen significantly in the time scales studied. At higher energies (400–500 eV), sputtering causes the Si(100) surface to become smoother on length scales smaller than 200 nm. © *2002 American Institute of Physics.* [DOI: 10.1063/1.1513655]

In recent years, surface morphology evolution during ion sputtering has received considerable experimental[1–10] and theoretical[11,12] attention. Bradley and Harper[11] showed that, under certain circumstances, surfaces undergoing off-axis sputter erosion exhibit instabilities to the formation of surface structures. While this model is essentially a continuum approach, it is also believed that the existence of step-edge diffusion barriers[1,13] or anisotropic surface diffusion[5] can generate surface structures through somewhat different mechanisms. Despite considerable progress in understanding morphology evolution during sputtering, much remains unknown and unexplored. For example, in the important technological case of Si(100) sputter erosion, existing studies[2,10] have focused largely on incident ion energies somewhat larger than those characteristic of industrial use (i.e. >750 eV as compared to Ar^+ energies less than 200 eV typical of ion energies in industrial plasma-based processes).

In this letter, we report a systematic investigation of Si(100) surface morphology evolution during normal-incidence Ar^+ sputtering at ion energies of 100–500 eV. In order to examine the kinetics in real time, *in situ* synchrotron-based grazing incidence small-angle x-ray scattering (GISAXS) was employed. The GISAXS technique measures the lateral correlations between height fluctuations on sample surfaces. Samples were also removed at key points in the process, as identified by the GISAXS measurements, for *ex situ* characterization with atomic force microscopy (AFM).

Silicon (100) wafers were initially cleaned either with a standard ''Radio Corporation of America'' regimen or with an acetone/alcohol treatment followed by an HF dip to remove the surface oxide. Samples treated in both manners showed similar surface morphology evolution during subsequent sputtering. Cleaned samples were immediately loaded into a UHV x-ray diffraction chamber (base pressure of 1.5×10^{-10} Torr) on beamline A2 of the Cornell High Energy Synchrotron Source (CHESS) for real-time x-ray studies.[1,14] Normal-incidence sputtering was performed with an Ion Tech (Veeco) rf ion-beam source providing Ar^+ ions with energies between 100 and 500 eV and an ion flux of 4×10^{14} ions/cm^2/s at the sample. Sputtering was examined at 100 eV, 150 eV, 200 eV, 300 eV, 350 eV, 400 eV, and 500 eV. The beam current was held fixed, independent of the beam energy.

Following an initial anneal to 500 °C to remove a surface film remaining after the cleaning procedure, samples were allowed to cool to temperatures of 55 °C–70 °C before sputtering experiments began. During sputtering, the sample temperature would systematically increase due to the relatively poor heat sinking of the sample in the experimental geometry. However, a separate study of the effects of heating the sample with a heater in the absence of the ion beam showed that the ion beam is playing a dominant role in determining the surface morphology evolution discussed here. Heating without the ion beam generally results in a decrease in the scattered intensity at the wave numbers of interest here.

GISAXS scans in the q_x direction (perpendicular to the sample normal z direction) were taken in real time during the erosion of the silicon surface. For small perpendicular momentum transfer, q_z, the GISAXS intensity is approximately proportional to the autocorrelation function of the position-dependent surface height. In all data presented here, $h_{\mathrm{rms}}q_z$

[a)]Electronic mail: ludwig@buphy.bu.edu
[b)]Current address: IQE Incorporated, 119 Technology Drive, Bethlehem, PA 18015.
[c)]Current address: Department of Physics, University of Vermont, Burlington, VT 05405-0125.

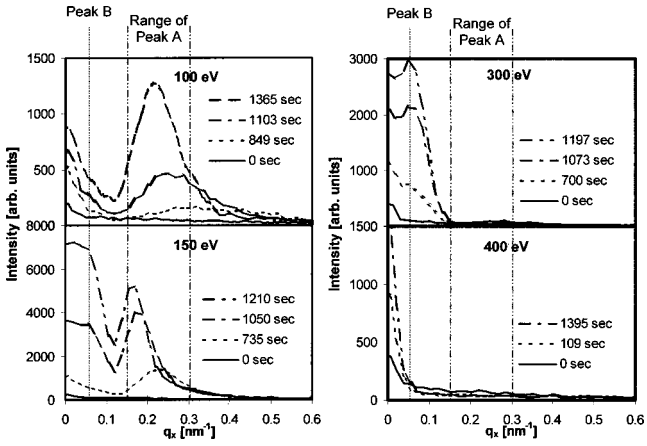

FIG. 1. Time evolution of the GISAXS patterns for sputtering at 100 eV, 150 eV, 300 eV, and 400 eV. The range of peak A and the position of peak B are marked. Peak A dominates at 100 eV while peak B dominates at 300 eV. At 400 eV, there is no clear development of lateral correlations on the length scales probed here (<200 nm).

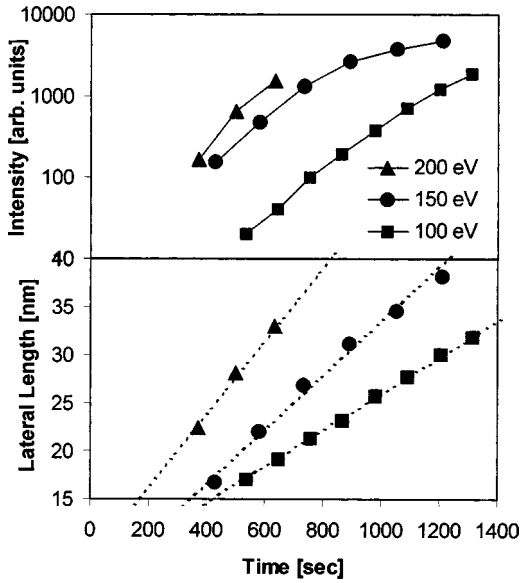

FIG. 2. Evolution of the peak A intensity and lateral length scale $d=2\pi/q_{\max}$. The dashed lines are fits to the lateral length scale evolution assuming a linear growth with a slope proportional to the ion-beam energy.

<0.3, where h_{rms} is the root-mean-square surface roughness over a 1 μm square as measured with *ex situ* AFM. Thus, we expect the small-q_z GISAXS interpretation to be at least qualitatively valid. The wave number resolution of the experimental apparatus was approximately $0.025\,\mathrm{nm}^{-1}$ full width at half maximum.

Typical GISAXS pattern evolution during the sputtering of a Si(100) surfaces with 100 eV, 150 eV, 300 eV, and 400 eV ion beams is shown in Fig. 1. The central peak at $q_x=0$ is due to the transverse tail of the specular reflection and is in some ways analogous to the direct beam in a conventional transmission small-angle scattering experiment. As can be seen in Fig. 1, at the lower sputtering energies, a peak forms at high wave numbers. As sputtering continues, the peak moves to lower wave numbers while continuing to narrow and grow in height. We will refer to this as peak ''A''. Simultaneously, another distinct peak (which we designate ''B'') forms at much lower wave numbers—near the central $q=0$ peak; this peak is dominant at 150 and 300 eV.

At higher beam energies (approximately 350–500 eV), no peaks are observed in the GISAXS patterns, as shown in the 400 eV data of Fig. 1. Moreover, after sputtering at these higher beam energies, scans along the specular rod (not shown here) suggest that the surface roughness is unchanged from that originally existing on the as-mounted sample. This is in distinct contrast to the situation with lower-energy ion beams where we observe a large drop in specular rod intensity associated with the growing surface roughness.

In order to quantify the evolutions of the peaks, GISAXS patterns were fit with the sum of three peaks, corresponding to peaks A and B and the central $q=0$ peak with a constant background. Preliminary fits indicated that, unlike the case of peak A, peak B did not appreciably move or narrow with increasing sputtering time. Therefore, in subsequent fits, its position and width were held fixed. Typical fit results for the time evolution of the intensity of peak A and associated lateral length scale positions $d=2\pi/q_{\max}$ from typical GISAXS patterns during sputtering at 100 eV, 150 eV, and 200 eV are shown in Fig. 2. The lateral length scales associated with peak A are 20–50 nm as compared to approximately 100 nm for peak B. The latter values are smaller by factors of 2–6 compared to the ripple wavelengths observed in the off-axis sputtering of Si(100) by Erlebacher *et al.*[2] using a somewhat higher Ar^+ beam energy (750 eV), higher fluxes (typically 4×10^{15} ions/cm^2/s) and higher temperatures ($>475\,^\circ$C). The increase in characteristic length scale is approximately linear in time for peak A with a slope proportional to sputtering energy in the Ar^+ energy range of 100–200 eV. The increase in intensity of peak A is nonlinear on the exponential scale, except perhaps at the earliest times. The limited intensity data would be consistent with a power-law temporal growth with a large exponent ($I\sim t^n$ with $n=4-5$).

In order to better understand the surface morphology evolution, *ex situ* AFM was performed to determine the real-space surface structure following selected sputtering treatments. Topographs were obtained using a Digital Instruments Nanoscope 2000 in tapping mode. Typical results are displayed in Fig. 3 for regimes in which peak A dominates the GISAXS pattern [Fig. 3(a)—100 eV for 1314 s] or peak B dominates the scattering [Fig. 3(b)—300 eV for 1203 s]. The rms height roughness as measured by the AFM is approximately 0.16 nm for the sample sputtered at 100 eV and 0.31 nm for the sample sputtered at 300 eV. Samples sputtered at higher energies showed no significant topograph morphology over a 1 μm^2 scan area, consistent with the GISAXS results. The lateral size scale of the features in the topograph of Fig. 3(a) is approximately 35–40 nm—in good agreement with the size scale found from peak A in the GISAXS pattern after sputtering this sample. The lateral size scale of the features in Fig. 3(b) is approximately 90–100 nm, again in good agreement with the size scale found from peak B in the GISAXS patterns. To be more quantitative about the comparison, we calculated the power spectral densities of the AFM topographs, i.e., the squares of the two-dimensional lateral Fourier transforms of the surface height distributions. As Fig. 4 shows, the AFM power spectral densities show striking agreement with the corresponding GISAXS patterns in Fig. 1. Beyond the obvious differences in the lateral and vertical scale of surface features, however, it is difficult to

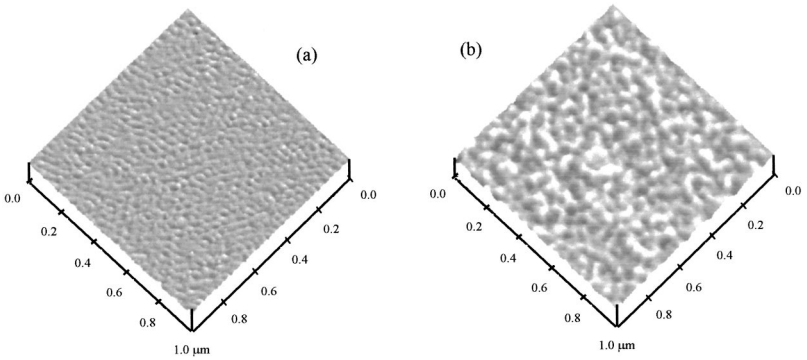

FIG. 3. AFM topographs of surfaces sputtered (a) with 100 eV ions for 1314 s and (b) with 300 eV ions for 1203 s. The vertical scale on each, corresponding from darkest to lightest tone is 5.0 nm.

pinpoint key structural differences between AFM topographs taken from samples sputtered with ion energies of 100–300 eV. Histograms of the AFM surface heights are nearly Gaussian out to at least the two-sigma level. Both topographs show significantly less order than reported, for instance, by Facsko *et al.*[3] in their study of GaSb.[3] Autocorrelation functions (not shown) typically exhibit only a single peak at approximately $d=2\pi/q_{\max}$.

In summation, GISAXS and AFM results show that, at technologically relevant Ar^+ beam energies of 100–300 eV, two distinct spatial structures develop simultaneously on the Si(100) surface and continue to roughen the surface with increasing beam exposure. One exhibits coarsening with a lateral length scale increasing linearly in time. The second exhibits a relatively constant lateral length scale with little, if any, dependence on beam energy. At higher beam energies of 400–500 eV, high wave number roughness is suppressed. The Bradley–Harper (BH) mechanism has previously been shown[2] to be operative on Si(100) for higher ion-beam energies, and the formation of dots has been reported using 1.2 keV Ar^+ ions.[10] While our results show no such dot formation at lower ion energies, strong correlations nonetheless develop with two distinct length and time scales. On metal surfaces, it is believed that step-edge barriers play a significant role in the sputter erosion process,[1,13] and it may be that they are also active on Si(100) at the lower ion energies used here. Thus, the two length scales observed may be due to two different processes operating simultaneously—the BH and step-edge mechanisms. Typically, the BH mechanism produces a stationary peak, consistent with the behavior of our peak B, while step-edge mechanisms produce peaks that indicate significant coarsening (i. e., shift to lower wave numbers with passing time), as does our peak A. Confirming the relevant mechanisms acting will require further experimentation. Clearly much remains to be learned about the behavior of surfaces undergoing low-energy ion sputtering.

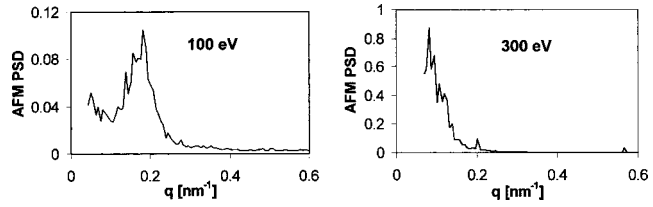

FIG. 4. AFM power spectral densities (PSD) for samples sputtered at 100 eV and 300 eV for 1314 s and 1203 s, respectively. These can be compared directly with the final GISAXS patterns in Fig. 1 for samples sputtered at these two energies. The AFM PSD do not have the peak at $q=0$ that exists in the GISAXS patterns due to the tail of the specular rod.

The authors thank Rajwinder Singh and Anlee Krupp of BU for help with the AFM, Xiaobo Wang, formerly of BU, for his help with x-ray data collection, and Steve Binari of the U.S. Naval Research Laboratory for the silicon samples used in this study. This work is partially supported by the NSF (Award No. DMR-0208011) and is based upon research conducted in part at the Cornell High Energy Synchrotron Source (CHESS), which is supported by the National Science Foundation under Award No. DMR-9713424.

[1] M. Ramana Murty, T. Curcic, A. Judy, B. Cooper, A. Woll, J. Brock, S. Kycia, and R. Headrick, Phys. Rev. Lett. **80**, 4713 (1998).
[2] J. Erlebacher, M. Aziz, E. Chason, M. Sinclair, and J. Floro, Phys. Rev. Lett. **82**, 2330 (1999).
[3] S. Facsko, T. Dekorsy, C. Koerdt, C. Trappe, H. Kurz, A. Vogt, and H. L. Hartnagel, Science **285**, 1551 (1999).
[4] E. Chason, T. M. Mayer, B. K. Kellerman, D. T. McIlroy, and A. J. Howard, Phys. Rev. Lett. **72**, 3040 (1994).
[5] S. Rusponi, C. Boragno, and U. Valbusa, Phys. Rev. Lett. **78**, 2795 (1997).
[6] E. A. Eklund, R. Bruinsma, J. Rudrick, and R. S. Williams, Phys. Rev. Lett. **67**, 1759 (1991).
[7] J. Krim, I. Heyvaert, C. Van Haesendock, and Y. Bruynseraede, Phys. Rev. Lett. **70**, 57 (1993).
[8] S. W. MacLaren, J. E. Baker, N. L. Finnegan, and C. M. Loxton, J. Vac. Sci. Technol. A **10**, 468 (1992).
[9] T. Michely, M. Kalff, G. Comsa, M. Strobel, and K.-H. Heinig, Phys. Rev. Lett. **86**, 2589 (2001).
[10] R. Gago, L. Vazquez, R. Cuerno, M. Varela, C. Ballesteros, and J. M. Albella, Appl. Phys. Lett. **78**, 3316 (2001).
[11] R. M. Bradley and J. M. E. Harper, J. Vac. Sci. Technol. A **6**, 2390 (1988).
[12] S. Park, B. Kahng, H. Jeong, and A.-L. Barabasi, Phys. Rev. Lett. **83**, 3486 (1999).
[13] O. Malis, J. D. Brock, R. L. Headrick, M.-S. Yi, and J. M. Pomeroy, Phys. Rev. B **66**, 035408 (2002).
[14] R. Headrick, K. Smolenski, A. Kazimirov, C. Liu, and A. Macrander, Rev. Sci. Instrum. **73**, 1479 (2002).